Papers Presented at the 24th EPS Conference on Controlled Fusion and Plasma Physics by the Alcator C-Mod Group (Berchtesgaden, Germany, 9 - 13 June 1997)

Plasma Science and Fusion Center
Massachusetts Institute of Technology
Cambridge, MA 02139

June, 1997

To be published in proceedings.

Papers Presented at the 24th EPS Conference
on Controlled Fusion and Plasma Physics by the Alcator C–Mod Group

Table of Contents

*Chalmers University, Goteborg Sweeden

Table of Contents (Cont'd.)

Fast Edge Mode observed during Enhanced D_α phase in Alcator C-Mod

I.H.Hutchinson, R.S.Granetz, A.Hubbard, J.A.Snipes, S.M.Wolfe

Plasma Science and Fusion Center, MIT, Cambridge, MA, USA

Abstract. An $n = 1$, $m = 4$ perturbation has been observed during the Enhanced-D_α H-mode phase on Alcator C-Mod. It is resonant just a few millimetres inside the separatrix and rotates extremely rapidly in the direction counter to the plasma current. This Fast Edge Mode is either an indicator of an extremely large negative radial electric field at the edge, or it is a mode rotating at about 4 times the estimated local diamagnetic velocity.

Introduction. The "Enhanced D_α" H-mode [1] on Alcator C-Mod occurs at high density and heating power, and appears to represent an attractive operational regime in which the impurity accumulation, characteristic of the ELM-free H-mode, is prevented without large ELMs. The energy confinement during D_α enhancement is slightly lower than ELM-free H-mode, but the edge particle confinement is much reduced. A search for the cause of the particle confinement reduction has revealed the presence in many enhanced D_α phases of an n=1 magnetic fluctuation with high frequency: 60 - 90 kHz. This "Fast Edge Mode" is unusual in comparison with other large-scale MHD fluctuations in that it rotates in the electron diamagnetic direction, or equivalently the counter-I_p direction. At present, these two characteristics (speed and direction of rotation) are regarded as the defining features of this low-m mode.

General observations. Fast edge modes sometimes occur in bursts lasting typically one millisecond that coincide with rises in the hydrogen light, and with slight rises in the plasma pressure observed by divertor embedded Langmuir probes at the separatrix. These bursts do not resemble ELMs of any previously identified type, being much more benign. Figure 1 shows an example of this behaviour. As indicated by the ECE T_e measurements, the fluctuation bursts show little or no (time-averaged) perturbation on the edge or central temperature and occur at a different time from the sawteeth. Some tendency has been observed for the bursts to occur shortly after sawteeth, when the edge temperature is near its maximum. In any case, the Fast Edge Modes occur interspersed with sawteeth whose precursors rotate in the opposite direction (co-I_p) with frequencies typically ten times smaller, thus demonstrating a "shear" in the mode rotation velocity.

Other Enhanced $D\alpha$ plasmas show quasi-continuous periods of Fast Edge Mode oscillations, and some show no clear coherent modes. Occasional Fast Edge Modes have been observed in what appear to be ELM-free H-modes. The magnetic fluctuations show no significant statistical coherence with the fluctuations observed on reflectometry[2], but both fluctuation levels are higher in Enhanced D_α phases.

Mode Structure Identification. Because of the very high frequency of the modes, their data are at present unaliased only on a subset of the magnetics diagnostics, primarily the coils mounted in the outboard limiter plus a few on the inboard wall. The
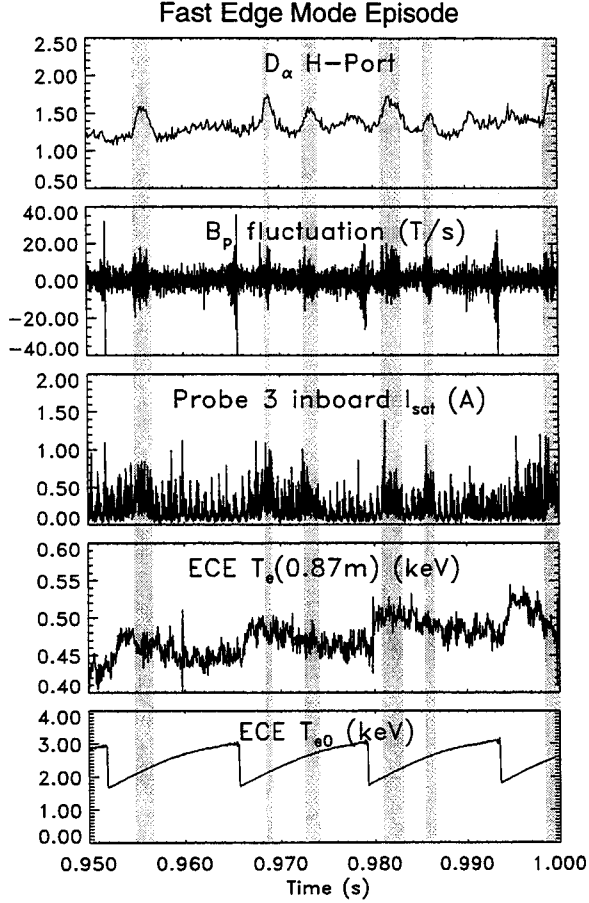
Figure 1: Bursts of Fast Edge Mode fluctuations appear on D_α, magnetics and separatrix probes but not ECE.
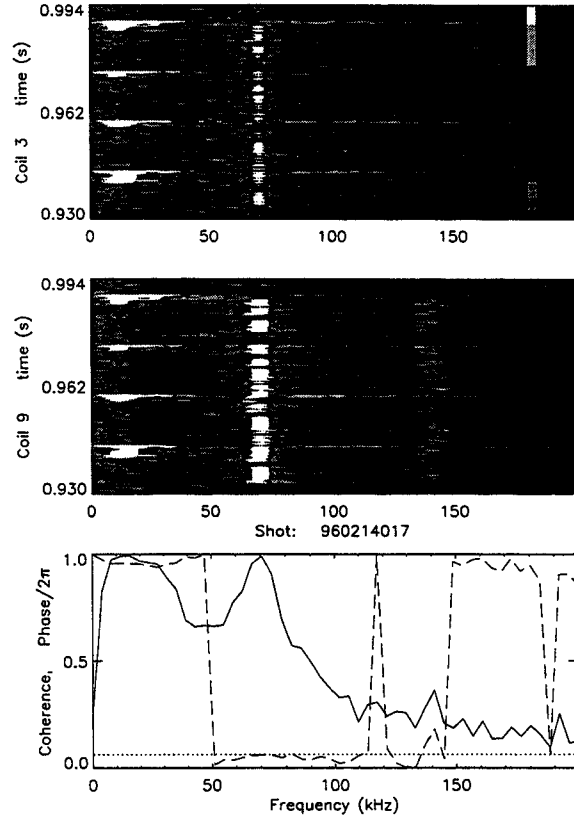

Figure 2: Frequency spectra evolution and cross coherence (solid) and phase (dashed) for magnetic coils separated by 10 degrees toroidally, during a continuous Fast Edge Mode.

limiter coils are installed in two limiters separated by a toroidal angle of 156 degrees. Each limiter has coils in pairs at the same poloidal position and separated by 10 degrees toroidally. This arrangement enables an unequivocal identification of the toroidal mode number of large coherent Fast Edge Modes as $n = 1$. In addition, spectrally resolved cross-correlation analysis is able to verify this identification in many cases when it is not visible by inspection. Figure 2 shows an example of this analysis. The spectra of two adjacent magnetic pick-up coils measuring $\dot{B}_\theta$ is shown together with their cross-coherence and cross-phase averaged over this time period. At the frequency of the Fast Edge Mode (70 kHz), the coherence is very high and the phase difference is about plus 10 degrees. For these two adjacent coils this indicates counter-rotation of an $n = 1$ mode. At the lower frequencies, bursts of sawtooth precursors can be seen. Their cross phase is minus 10 degrees (equivalent to plus 350 degrees), showing opposite (i.e. co-) rotation.

Because the plasma is strongly shaped, naive "poloidal angle" fits of the poloidal mode structure are misleading, and because of the sparseness of the fast magnetics data in poloidal angle, it is not possible simply to count nodes and antinodes. Instead, a value of safety factor, q_s, is specified, and on the flux surface of the equilibrium reconstruction

2

corresponding to this safety factor, the field-line is followed in 3-dimensions around the torus, tracing out a poloidal contour. At intervals on this contour corresponding to constant increments of toroidal angle, and hence of toroidal mode phase difference at constant poloidal position, are placed filaments with current proportional to $\exp(-i\delta\phi)$, where $\delta\phi$ is the phase difference. The poloidal projection then has filaments with positions and phases corresponding to modelling the perturbation as currents following field-lines on this rational surface. The values of the field perturbation arising at the magnetic measurements from these filaments are then calculated and compared with the experimental observations. (The influence of the conducting vacuum vessel is ignored at present). The resonant q_s is that which gives the best fit by this process. Figure 3 gives an example.

The measured values of the amplitudes and phases of the mode at the measurements can sometimes be obtained by inspection. However, when their amplitude is small, statistical methods are needed to recover the corresponding values from the noise. The approach used is to form the cross correlation matrix for all the relevant measurements in the frequency band of interest. The largest principle component (i.e. eigenvector with largest eigenvalue) of this matrix is then taken as the experimental mode structure.

For the cases analysed so far, the fast edge mode is found to be quite well fitted by the field-aligned current model with $m = 4$ (and $n = 1$). The coils on the outboard limiters are by themselves unable to distinguish between $m = 1 - 5$ because it is observed that the modelled phase variation across them is hardly different for the different poloidal mode numbers. This is a feature of the field structure as a function of flux surface. Actually

Figure 3: Fit of perturbation mode (stick arrows) to observed magnetics (filled arrows). The amplitude and phase at the probe locations are shown by arrow size and orientation. The second limiter coils are shown shifted right. The model filament phase is also given by arrow orientation on the resonant flux surface.

there is a small discrepancy observable in Fig 3, in that the modelled phase difference from top to bottom of the limiter is $\sim 30\%$ less than the measured phase difference (for all modelled m-numbers). This is believed to be because the mode does not exactly follow the field-line in shaped-cross-section plasmas; a small amount of field bending is preferred. The critical measurements for mode identification, then, are the inboard
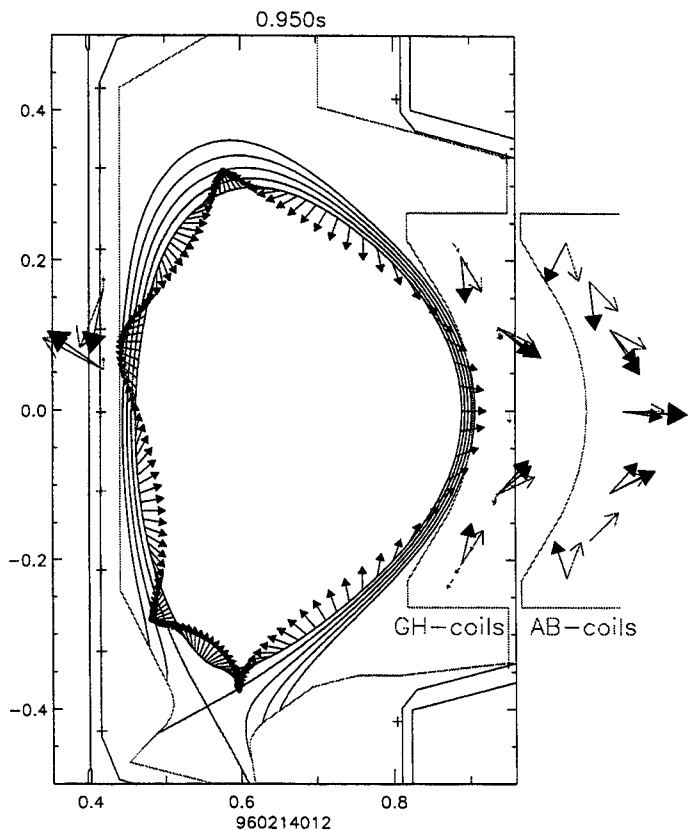
3

coils. Their amplitude in addition to their phase, is quite well matched (by $m = 4$). This fact indicates there is no appreciable "ballooning" character to the mode.

Analysis and Discussion. The Fast Edge Mode is clearly different from the type III ELM precursors previously observed on Alcator C-Mod [3] and elsewhere, and from, for example, the "Quasi Coherent Mode" observed on PDX [4] in that it has $n = 1$, not large ($n \sim 10$ in ref [3]).

The $q = 4$ surface is only 4 mm from the separatrix, at the midplane, in these plasmas, so this mode is resonant within the steep gradient region of the H-mode "pedestal" or thermal barrier. The mode amplitude is quite small. The typical poloidal field perturbation at the coils is $\sim 2 \times 10^{-5}$ T. A crude estimate of the size of any magnetic island at the resonant surface may be obtained by supposing that a radial field of this magnitude exists on the resonant surface. In that case an island width of only ~ 1 mm would result using the standard island width formula $4\sqrt{(rq_s \tilde{B}_r / m q_s' B_p)}$.

The frequency and mode number of the mode tells us its velocity perpendicular to the field, assuming the mode is essentially field-aligned. If the velocity were all toroidal, it would be typically 4×10^5 m/s; whereas if it were all poloidal it would be 5×10^4 m/s. These speeds should be compared with the typical ion sound-speed of $\sim 10^5$ m/s in the vicinity of the mode rational surface. It seems unlikely that the rotation could be toroidal; if it were, it would be at about Mach 4.

The speed of the mode may be discussed in terms of the standard radial pressure balance (for ions) $E_r = (1/Zen_i)\partial p_i / \partial r - v_{ip}B_\phi + v_{i\phi}B_p$, where E_r is the radial electric field, n_i, p_i and v_i are the ion density, pressure and velocity. If we suppose the mode rotation to be due to $E \wedge B$ drift (the E_r term) alone, we deduce an extremely large *equivalent* negative radial electric field, $E_r \approx -350$ kV/m.

The mode probably is not at rest in the frame moving at the $E \wedge B$ velocity. Resistive modes tend to move with the electron drift velocity, which is moving relative to this frame at the electron diamagnetic velocity. Our knowledge of the diamagnetic drift velocity in the H-mode edge barrier is limited so far by insufficient spatial resolution (about 1 cm) of diagnostics. But even a generous estimate of about 0.5 keV in 0.5 cm (100 kV/m) is about four times too low to account for the observed rotation in terms of diamagnetic drifts. Moreover, if the velocity were to be attributed to pressure gradients – much steeper than presently estimated – the gradients would have to exceed the first ballooning limit by a substantial factor.

The Fast Edge Modes then, are highly edge-localized, n=1, perturbations whose rapid rotation shows either that they exist in a region with a very large negative radial electric field, or that the mode is a peculiar, as yet unidentified, instability.

References.
[1] Y. Takase *et al*, Phys. Plasmas **4** 1647 (1997).
[2] P. C. Stek *Reflectometry Measurements on Alcator C-Mod* PhD Thesis, MIT, (1997).
[3] J. A. Snipes *et al*, Plasma Phys. Control. Fusion **38** 1127 (1996).
[4] R. Slusher *et al*, Phys. Rev. Lett. **53** 667 (1984).

4

SOL Power and Pressure Balance in Alcator C-Mod

C S Pitcher, J A Goetz, B LaBombard and B Lipschultz

MIT, Plasma Science and Fusion Center, NW17, Cambridge, MA, 02139, USA

1. Introduction

In this paper we compare the results of a simple model of scrape-off layer (SOL) power and pressure balance, with detailed plasma measurements in the Alcator C-Mod tokamak. The model is based on the commonly used 'Two-Point Model', but includes significant additions (described in detail in a recent review article [1]). The present paper should be considered as a companion to an earlier publication [2], where similar data from the ASDEX-Upgrade tokamak was presented.

2. Power Balance

We assume that power flows along field lines in the SOL with a density q_u from the upstream stagnation location to the divertor by electron heat conduction,

$$T_u^{7/2} - T_t^{7/2} \simeq \frac{7 q_u L}{2 \kappa_0} \tag{1}$$

where L is the connection length ($\simeq 8m$), T is the plasma temperature (we assume $T_i = T_e$), κ_0 is a constant and 'u' and 't' denote the upstream (we assume outer mid-plane) and (outer) target plate locations, respectively.

In Eqn. 1 we have assumed that the parallel power is nearly constant over most of the length of the flux tube. This is approximately valid, as detailed calculations have indicated, even in cases with high radiation on open surfaces, since such radiation tends to be localized near the divertor where densities are elevated. Although simple analytic estimates of such radiative loss based on 1-D modelling can be used [1,2], assuming for example, constant impurity radiation coefficients and impurity fractions, the associated error is significantly larger than other uncertainties implicit in the simple modelling. We therefore take the experimentally determined radiative loss near the divertor as an input to the model, i.e. q_{rad}.

The boundary condition at the target plate is

$$q_t = n_t c_{St}(\gamma T_t + \epsilon_{pot}) \tag{2}$$

where, q_t is the parallel power density at the target plate ($q_t = q_u - q_{rad}$), c_{St} is the ion acoustic speed and $\gamma = 7$ is the sheath power transmission factor. ϵ_{pot} is the potential energy associated with each ion reaching the plate, including atomic and molecular recombination ($\epsilon_{pot} \simeq 16eV$).

3. Neutral Dynamics

We allow for the loss of plasma pressure by ion neutral friction in a thin recycling region close to the divertor plate. The pressure loss factor, f_m, is given by,

$$f_m \equiv \frac{2 n_t T_t}{n_u T_u} = 2\left(\frac{\alpha}{\alpha + 1}\right)^{\frac{\alpha+1}{2}} \tag{3}$$

where,

$$\alpha \equiv \frac{<\sigma v>_i}{<\sigma v>_i + <\sigma v>_m} = f(T_t) \tag{4}$$

where $<\sigma v>$ are the rate coefficients for ionization (i) and momentum loss (m), including both elastic and charge-exchange collisions, given by [3]. Eqns. 3 and 4 were originally derived for gas discharge theory [4]. We assume an isothermal plasma temperature in the recycle region.

The neutral density in the recycle region n_H is related to the parallel scale-length of the region L_H, according to [1],

$$n_H L_H = F(T_t) \equiv \frac{c_{St}}{<\sigma v>_i + <\sigma v>_m} \left(\frac{\alpha+1}{\alpha^{1/2}} \arctan \alpha^{-1/2} - 1 \right) \tag{5}$$

The parallel scale-length is determined using,

$$L_H = \frac{\lambda_H}{sin\theta} \tag{6}$$

where θ is the field line pitch angle at the plate and λ_H is the poloidal penetration distance from the plate of recycled neutral atoms based on charge-exchange diffusion [5],

$$\lambda_H = \left(\frac{8T_t}{3\pi m <\sigma v>_i <\sigma v>_m} \right)^{1/2} \frac{1}{n_r} \tag{7}$$

where $n_r = 2n_t/f_m$ is the density at the entrance of the recycle region.

Typically in experiments, rather than n_H in the plasma, one diagnoses the molecular gas adjacent to the divertor fan,

$$\phi_{mol} = \frac{\phi_H}{2} = \frac{1}{8} n_H \bar{c}_H \tag{8}$$

where the ϕ's are the molecular ('mol') and atomic ('H') flux densities and $\bar{c}_H$ is the mean thermal speed of atoms in the fan based on the plasma temperature T_t. We have assumed that atom fluxes out of the fan are balanced by molecular fluxes back into the fan and that other net particles sources and sinks are small in comparison to this exchange.

4. Experiment

The model is compared with experimental results from the Alcator C-Mod tokamak. The SOL plasma density and temperature are measured at the upstream and outer target plate locations with Langmuir probes. The molecular flux density outside of the plasma fan in the divertor is determined using an absolutely calibrated capacitance manometer. The radiated power in the divertor is deduced using multiple chords of bolometer cameras. The experimental results presented here consist of Ohmic discharges at various densities without boronization with $I_p = 0.8MA$, $B_t = 5.4T$ and vertical outer plate geometry.

In Fig. 1 we compare the experimentally determined pressure loss factor f_m at the outer plate on a number of flux surfaces (denoted by their ρ values, mapped to the outside mid-plane) with the prediction of Eqns. 3 and 4. Reasonable agreement between model and experiment is obtained, with strong pressure loss for $T_t < 5eV$ and no pressure loss for $T_t > 10eV$. In particular, the rapid decrease in f_m at low T_t is strong evidence that atomic physics processess are responsible. In the case of neutral friction, this results from the rapid decrease in ionization rate $<\sigma v>_i$ compared with charge-exchange rate $<\sigma v>_m$. Fig. 1, however, may also be consistent with other atomic processes being responsible, for example, volume recombination, which

6

also has a strong temperature dependence and whose signature has recently been observed in C-Mod [6,7].

The fact that f_m values on different fluxes surfaces are coincident, is perhaps surprising, given the 1-D nature of the model. This is reasonable, however, since plasma flow in the recycling region is primarily along field lines, from ionization source close to the plate to the surface sink, with cross-field transport of plasma being of minor importance.

The full model is now compared with experiment in Fig. 2, as a function of line-average density $\bar{n}_e$ for conditions on a flux surface near the separatrix, $\rho = 1mm$. Two fitting parameters are used in this modelling – the radiated power, as mentioned above, is taken from experiment, and the relation between the upstream density and $\bar{n}_e$, where we make the approximation $n_u = \bar{n}_e/3$. Thus, the 'good fit' between model and experiment in Figs. 2a and 2b is artificial. From global power balance and measurements of the mid-plane radial plasma profiles, $q_u \simeq 75 MW m^{-2}$, which is assumed fixed in the modelling, approximately consistent with experiment.

Fig. 2c, 2d, 2e give the model prediction and experimental results for the target plate conditions, n_t, T_t and p_t, and the upstream conditions T_u and p_u, where $p_{t,u}$ are the total electron pressures. The data clearly exhibits three characteristic regimes – the linear/sheath-limited regime at low density, the high recycling regime at moderate density and the detached regime at high density [1,8]. The linear regime has nearly isothermal conditions between the upstream location and the target plate, with $n_t \propto \bar{n}_e$ and no pressure loss along field lines. In the high recycling, large parallel temperature gradients develop, the target density rises rapidly with discharge density, $n_t \propto \bar{n}_e^3$, and no pressure loss is observed, since $T_t > 10eV$. In the detached regime, the T_t drops below 5 eV and significant pressure loss becomes possible, which results in a 'roll-over' of the target plate density n_t.

The model also gives the molecular flux density outside of the fan, ϕ_{mol}. One notes this continues to rise, throughout all regimes, following in the linear regime $\phi_{mol} \propto \bar{n}_e$, $\phi_{mol} \propto \bar{n}_e^3$ in the high recycling and continuing to rise in the detached regime. It may be, at first sight, surprising that atomic and molecular fluxes should continue to increase in the detached regime, despite a decrease in plasma ion density (and fluxes) at the target plate. The high neutral density is explained, after consideration of ion particle continuity, by the need to supply enough ionization in the face of a strong decrease in the ionization rate at low plasma temperatures [1,9].

References

[1] C S Pitcher and P C Stangeby, Plas Phys Contr Fus (1997), in press

[2] C S Pitcher et al, EPS Proceedings (Bournemouth, 1995) III-245

[3] R K Janev et al, Elem Proc in H-He Plas, Springer-Verlag, Berlin (1987)

[4] S A Self and H N Ewald, Phys. Fluids 9 (1966) 2486.

[5] B Lehnert, Physica Scripta 12 (1975) 327

[6] D Lumma et al, Phys Plas (1997), in press

[7] J L Terry et al, these proceedings

[8] B LaBombard et al, Phys Plas 2 (1995) 2242

[9] A Niemczewski et al 37 (1997) 151

Fig. 1

Fig. 2

f_m

model

ρ (mm)
+ 1
◇ 2
△ 3
□ 4.5
× 6.5

T_t (eV)

linear │ high recycle │ detached

linear │ high recycle │ detached

(a) $P_{rad,div} / P_{SOL}$

(b) n_u (m^{-3})

(c) n_t (m^{-3})

(d) T_e (eV) — u, t

(e) p_e (Pa) — u, t

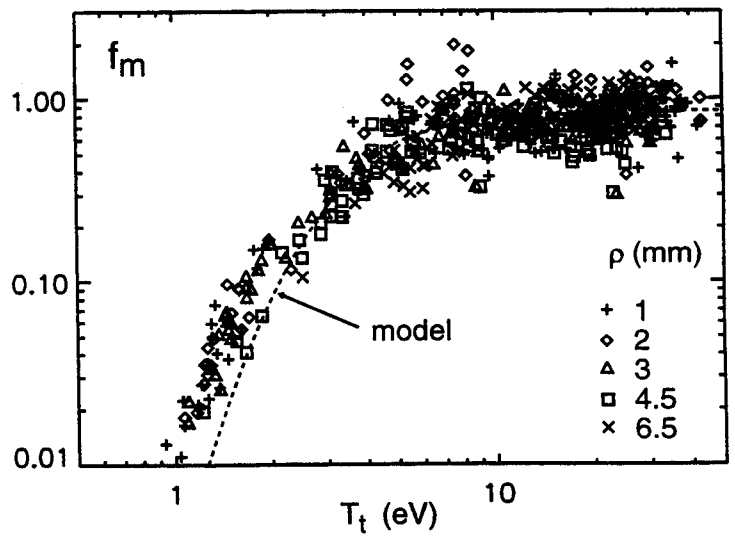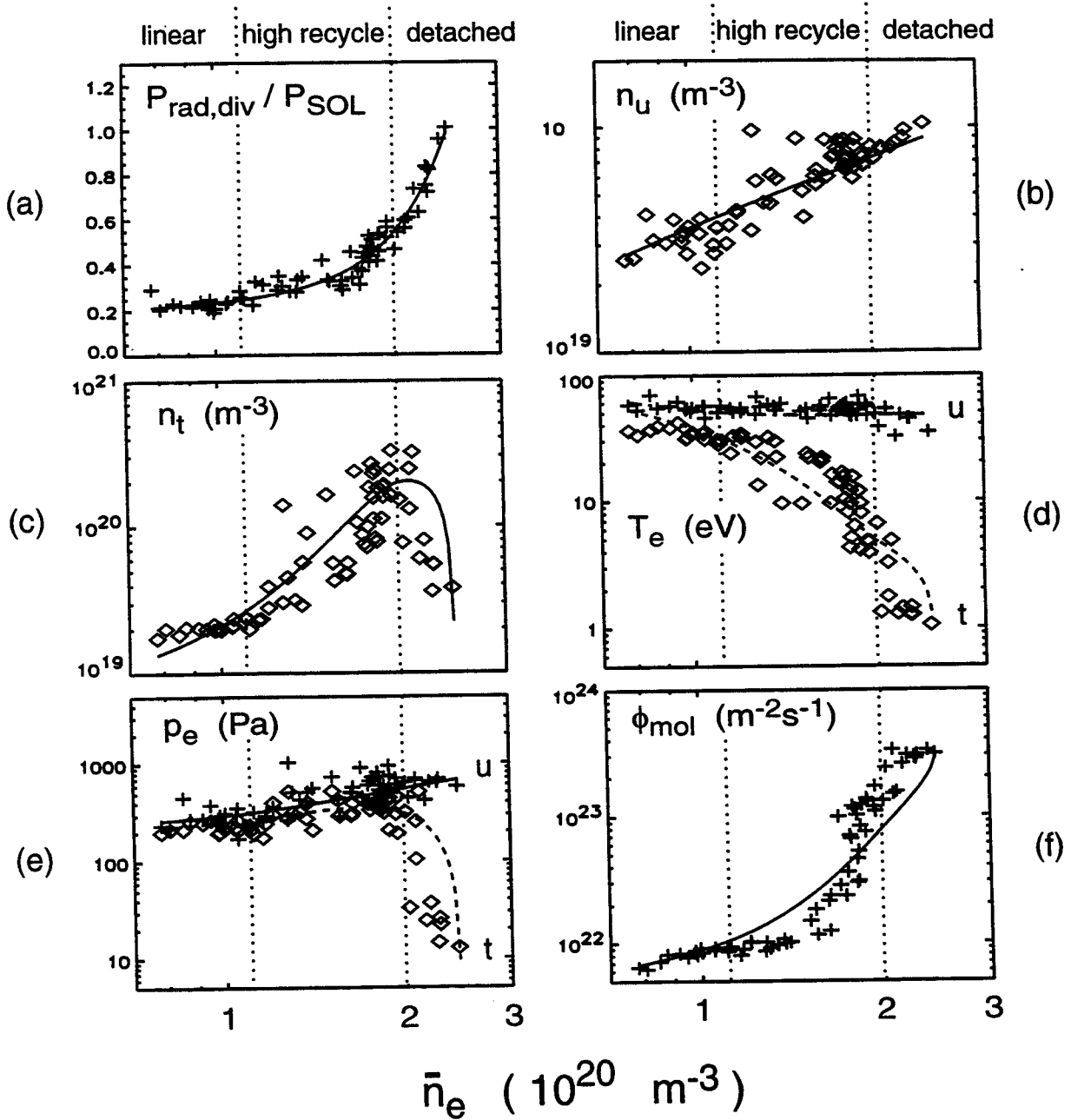(f) ϕ_{mol} (m^{-2}s^{-1})

$\bar{n}_e$ (10^{20} m^{-3})

Reversed Shear Experiments in Alcator C-Mod with Current Ramp and ICRF Heating*

M. Porkolab, R. Boivin, P.T. Bonoli, C. Fiore, M. Greenwald, A. Hubbard,
I.H. Hutchinson, Y. In, E. Marmar, P. O'Shea, J. Ramos, J. Rice, J.C. Rost,
J.A. Schachter, J. Snipes, Y. Takase, S.M. Wolfe, and the Alcator C-Mod Group
MIT Plasma Science and Fusion Center, Cambridge, MA,02139, USA
A. Bondeson, Chalmers University, Goteborg, Sweden

Initial scoping experiments were performed to obtain the enhanced reversed shear (ERS) mode in Alcator C-Mod[1] using current ramp and early ICRF heating in the D(H) minority heating regime. Alcator C-Mod is a relatively modest size ($R = 0.67$ m, $a = 0.22$ m), but high power density and high field ($B_t \leq 9.0$ T, $I_p \leq 1.5$ MA) tokamak with a divertor and substantial elongation ($\kappa \leq 1.8$), which should provide valuable data regarding ERS operation with purely RF heating in a plasma with comparable T_e and T_i. In these experiments up to 2 MW of ICRF power at 80 MHz were injected using a pair of two strap antennas, each phased at 180° between adjacent straps[2]. The volumetric power density exceeded 2 MW/m^3, and the surface power density exceeds the H-mode threshold in the steady current phase of the discharge beyond the first sawtooth crash at 0.23 s, a substantial fraction of the resistive skin time. Typical plasma parameters at the end of the 0.23 s sawtooth free period were $\bar{n}_e = 1 \times 10^{20}$ m^{-3}, $B_t = 5.3$ T, $T_{e0} = 5$ keV, $T_{i0} = 2.5$ keV, $n_H/n_e \simeq 0.04 - 0.05$, and $I_p = 0.8$ MA. Calculations with a combined Fokker Planck - ICRF heating code FPPRF [3] indicate for these parameters approximately 70% of the rf power carried by the minority (H) tail is transferred collisionally to the background electrons. During the initial plasma phase ($t \lesssim 0.12$ s), the coupled power from the two ICRF transmitters varies between 0.8 - 1.8 MW. Beyond this time, both transmitters couple well into the target plasma, providing a continuous power of 1.8 MW. During the ramping phase, $0.08 - 0.1$ s into the discharge initiation phase, MHD oscillations were observed on both poloidal field pick-up coils and ECE diagnostics. The short bursts of coherent low frequency (1 − 10 kHz) MHD oscillations lasting for 10 ms were observed just as $q_{\psi_{95}}$ dropped below 5. The correlated oscillations were observed on several ECE grating polychromator signals which measures T_e at 9 radial locations along the midplane. The diagnostic is sampled at 20 kHz and has a radial resolution of 0.9 cm, with 2.0 cm separation between channels. As shown in Fig. 1, clear perturbations can be seen on several channels during the current rise, indicating a relatively wide mode structure, typically in the range $0.4 \leq r/a \leq 0.9$. The peak in the fluctuations varies from $r/a = 0.75 - 0.85$ (see Fig. 2). Equilibrium reconstruction using the EFIT code [4] was also done in an attempt to establish the main plasma equilibrium quantities, including the q-profiles. At least three distinct equilibria were established, each with somewhat different current and q-profiles. These q-profiles are also plotted in Fig. 2, two of them being a clear reverse shear profile
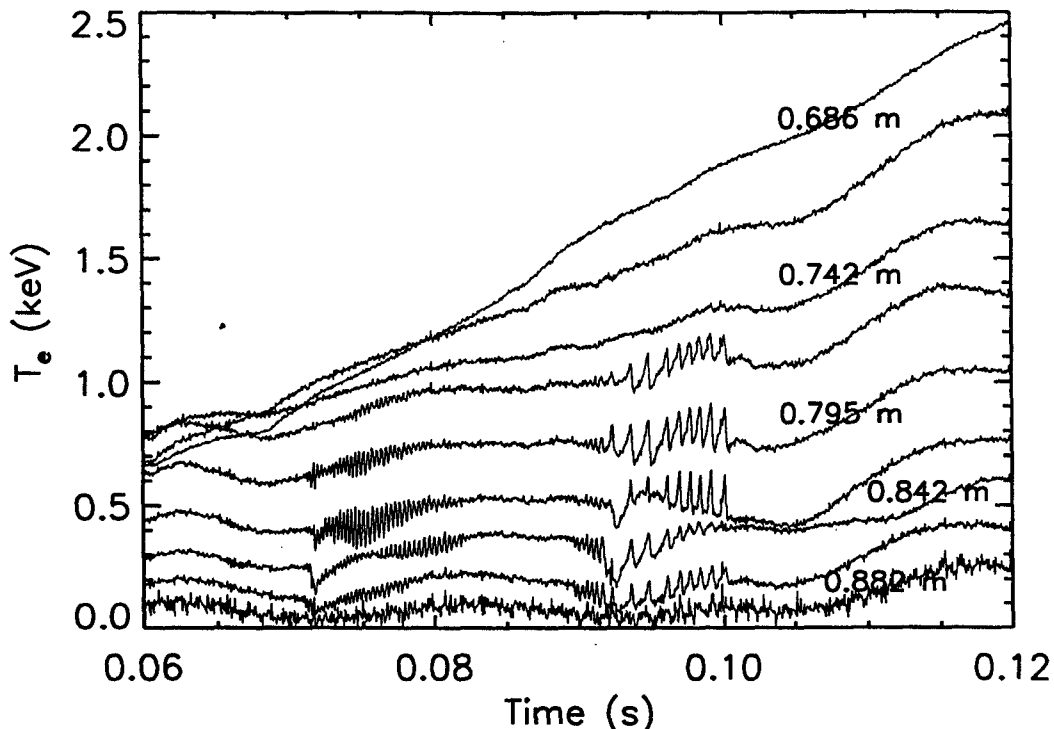
Figure 1: Electron temperature versus time from GPC for C-Mod Shot 960223047.

with $q_0 = 4.2 - 4.7$, $q_{min} = 3.2 - 3.1$, $q_{95} = 4.5$, while the third profile tended to be flat in the inner half of the plasma, with $q_{min} = 3.0$, and $q_{95} = 4.5$. One of the reversed shear q-profiles, with $q_0 = 4.7$, $q_{min} \simeq 3.1$ was characterized by substantial edge current pedestals, with significant MHD stability consequences, as is discussed below.

The poloidal and toroidal mode numbers of the oscillations were determined by comparing the measured phase of the oscillations on poloidal field pick-up coil signals from the outboard limiter and the inner wall at different toroidal locations. The mode numbers were found to be $m = 5$, $n = 1$ on shot 960223047 at both 0.08 s and 0.09 s, which corresponds to a flux surface that passes from $r/a = 0.96$ to $r/a \sim 1$ as the current rises. A current filament code was also run to compare the measured phases with the expected phases from a perturbation at the $q = 5$ surface and good agreement was found between the expected and measured phases.

We have carried out a detailed MHD analysis of the 960223047 discharge during its current ramp phase in an attempt to explain the observed $n = 1$ fluctuations. We have concentrated on a time point of 0.092 s that corresponds to the beginning of the second burst of MHD activity. The MHD stabiliy has been investigated with the linear code MARS [5] for resistive modes. It is important to realize that the MHD stability results are sensitive to equilibrium details that cannot be resolved with the available diagnostics of pressure and current profiles. In particular significant uncertainties exist regarding the

inner shape of the current or q-profiles, and regarding the precise values of the current density and its gradient at the plasma edge. For the case under consideration we have investigated all three different EFIT equilibria shown in Fig. 2.
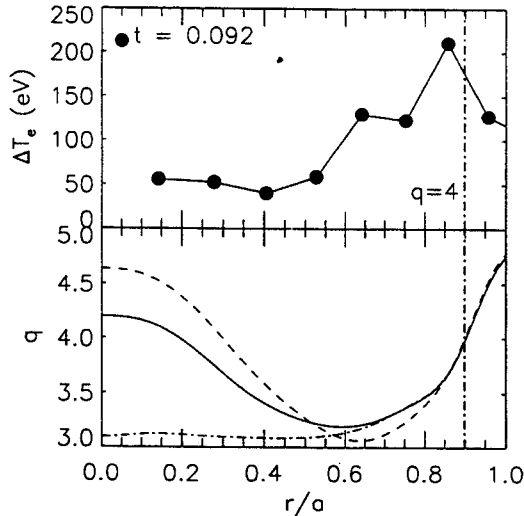

Figure 2: Electron temperature fluctuation profile for Shot 960223047 (top curve). Profiles of safety factor (q) for three distinct EFIT equilibrium reconstructions of Shot 960223047 (bottom curves).
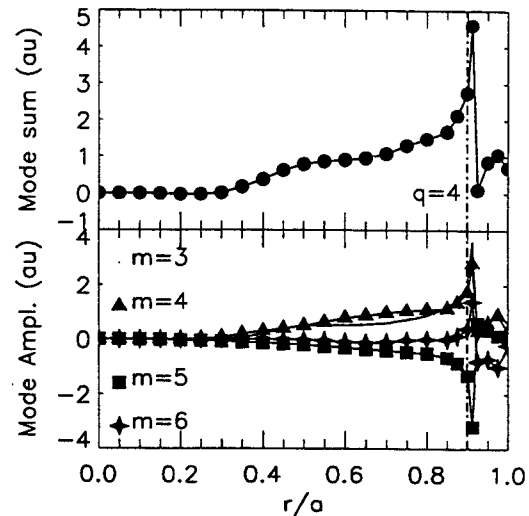
Figure 3: Resistive MHD mode analysis for non-monotonic q-profile in Fig. 2 with $q_0 = 4.2$. Eigenfunction for $n = 1$ resistive mode.

The MHD analysis of the first equilibrium (flat q-profile) using the MARS code yields an $n = 1$ resistive (tearing) instability localized at the $q = 4$ mode resonant surface near the plasma edge. The growth rate of this mode is low, with an estimated e-folding time of the order of 10 ms. This result should be taken only as a rough approximation because the MARS code uses only a simple expression for the temperature profile of the form $(T/T_0) = (p/p_0)^\alpha$, $(n/n_0) = (p/p_0)^{1-\alpha}$, and $Z_{eff} = 1$ when evaluating the plasma resistivity. In our calculation we took the experimental values for $T_0 = 1.6$ keV and $n_0 = 0.7 \times 10^{20}$ m^{-3}, and a simple guess $\alpha = 0.6$. Thus this model may yield a value of the plasma resistivity at the edge near the $q = 4$ mode resonant surface significantly different from the actual one . The second equilibrium is found unstable to a very similar $n = 1$ resistive mode whose eigenfunction is (with $q_0 = 4.2$) diplayed in Fig. 3. This is a single tearing mode localized at the outer $q = 4$ resonant resonant surface, despite the fact that this equilibrium has a non-monotonic q-profile with two $q = 4$ surfaces within the plasma. The absence of a double tearing mode can be understood because the two $q = 4$ surfaces are far apart and the inner one is in a high temperature region, so that the resistive mode only grows at the colder, outer resonant surface. The growth rate of this instability is

very close to the one in the first equilibrium where q is monotonic.. The structure of the eigenfunction is also very similar but the enhancement of the $m = 3$ component in the central region of flat $q \simeq 3$ of the first equilibrium is now absent. We can conclude that the modification of the internal current density profile from the first EFIT reconstruction to the second one has little effect on this resistive mode.

The third equilibrium ($q_0 = 4.7$) is found unstable to an $n = 1$ ideal external mode, that appears to be driven by the larger edge current density (not shown here) and current density gradient of this equilibrium fit, combined with the presence of a $q = 5$ mode resonant surface in the vacuum just outside the plasma. This ideal mode has a growth rate about 100 times faster than those of the resistive modes in the first two equilibria, with an e-folding time of the order of 0.1 ms independent of the resistivity. Its eigenfunction peaks near the outside vacuum region.

Comparison with the signature of the experimentally observed fluctuations is not conclusive. The fact that the observed fluctuation amplitudes seem to exhibit a maximum about $q = 4$, favors the interpretation in terms of the resistive mode rather than the edge kink-mode. The discharge is not disrupted, and the main impact of these modes is that the electron temperature is "clamped" in regions of large mode amplitudes. These modes become stabilized as the discharge evolves toward higher temperatures.

In these preliminary experiments no evidence of the ERS confinement regime was observed yet. As the discharge evolves, at ~ 0.15 s high frequency, ($\sim 300 - 400$ kHz) narrow bandwidth modes were observed, which are believed to be TAE modes driven by the hydrogen minority tail. Future experiments, including $D(^3He)$ minority heating and pellet injection, should favor increased ion heating and hence the enhanced reversed shear (ERS) mode. In addition, off-axis mode-conversion current drive will be carried out in an attempt to "clamp" the reversed shear equilibrium.

References

[1] HUTCHINSON, I.H., et al., Phys. Plasmas **1**, 1511 (1994).

[2] TAKASE, Y., et al., *Proc. 14th IEEE/NPSS Symp. Fusion Engineering* (San Diego, CA, 1992) p. 118.

[3] HAMMETT, G.W., "Fast Ion Studies of Ion Cyclotron Heating in the PLT Tomamak", PhD Diss., University Microfilms Int. No. GAX86-12694, Princeton University (1986).

[4] LAO, L.L., et al., Nucl. Fusion **30**, 1035 (1990).

[5] BONDESON, A., et al., Phys. Fluids B, 1989 (1992).

Enhanced D_α H-modes in Alcator C-Mod

J. A. Snipes, R. Boivin, C. Fiore, J. A. Goetz, A. Hubbard, I. H. Hutchinson,
J. Irby, B. LaBombard, B. Lipschultz, E. S. Marmar, J. Rice,
P. C. Stek, Y. Takase, J. L. Terry, S. M. Wolfe

MIT Plasma Science and Fusion Center, Cambridge, MA USA

Introduction A new and potentially reactor relevant high confinement regime has been found on Alcator C-Mod at high electron density ($\bar{n}_e > 2 \times 10^{20}$ m^{-3}) with ICRF heating, called the Enhanced D_α H-mode (EDA H-mode) [1]. These H-modes reach a steady state density and total radiated power, yet remain free of discrete ELMs throughout the ICRF heating phase. The D_α emission drops initially as the plasma enters H-mode, then rises rapidly, often returning to L-mode levels at the midplane and in the divertor as the density reaches a steady state. The energy confinement of Enhanced D_α H-modes is slightly lower than that of the best ELM-free H-modes, but can still reach and maintain confinement enhancement factors up to two relative to L-mode. High frequency (50 - 100 kHz) density and magnetic fluctuations are often observed during EDA H-modes.

Method of Operation Enhanced D_α H-modes were first obtained after closing off some divertor bypass leaks, which increased the divertor/midplane neutral compression ratio from a range of 10-100 to a range of 50-250 in H-mode. The first moderately enhanced D_α H-modes were obtained before the machine was boronized by operating at high density ($\bar{n}_e > 2.5 \times 10^{20}$ m^{-3}) and high ICRF heating power ($P_{ICRF} > 2.5$ MW) with strong gas puffing.

After boronization with B_2D_6, EDA H-modes were obtained at high density without strong gas puffing. While high ICRF power is usually required to achieve EDA H-mode, some were achieved immediately after boronization with $P_{ICRF} < 1$ MW. The divertor pressure in EDA H-mode is usually 2 - 10 Pa, but after a fresh boronization, EDA H-modes can occur with divertor pressures from 0.25 - 1 Pa. Boronization widens the operational range of EDA H-mode through lower core radiation and increased particle inventory.

Particle and Energy Confinement EDA H-modes have somewhat lower core particle and energy confinement than ELM-free H-modes in C-Mod. The core impurity particle confinement time was measured with trace scandium injection during an ELM-free H-mode that became an EDA H-mode before the scandium left the plasma (Fig. 1) . In the ELM-free phase, the scandium did not decay, indicating an impurity confinement time much greater

13

than 0.2 sec. In the Enhanced D_α phase, the scandium left the plasma with a characteristic decay time of 0.1 sec. By comparison, in the L-mode phase, the scandium decay time was about 30 msec. So, in EDA H-mode, the core impurity confinement time is about three times higher than L-mode, but at least two times lower than ELM-free H-mode.

The reduced particle confinement of EDA H-mode relative to ELM-free H-mode leads to reduced impurity accumulation in EDA H-mode. The radiated power saturates in EDA H-mode at a

Fig. 1. Scandium injection at 0.7 sec to measure particle confinement in ELM-free and EDA H-mode.

steady state value with $0.2 < P_{rad}/P_{tot} < 0.6$ rather than continuing to increase as in ELM-free H-mode (Fig. 2). The total radiated power profile across the main plasma, measured by bolometers, is substantially lower in EDA H-mode than in ELM-free H-mode. By contrast, the divertor radiation is substantially higher in EDA H-mode than in ELM-free H-mode. Z_{eff} is also lower in EDA H-mode than in ELM-free H-mode.

The peak energy confinement in EDA H-mode is generally slightly lower than in ELM-free H-mode, but can still reach 2 × L-mode. Values of the thermal energy confinement time in EDA H-mode $\tau_{Eth}^{EDA} > 60$ msec have been achieved compared to ELM-free values up to $\tau_{Eth}^{EFH} \approx 80$ msec. The advantage of EDA H-mode over ELM-free H-mode is that the confinement remains high in steady state for as long as the ICRF pulse because the impurities do not accumulate and radiate away the thermal energy. This is accomplished without the large perturbations of Type I ELMs. So, EDA H-mode has the improved confinement of Type I ELMy H-mode, without the problems associated with large ELMs.

Divertor Physics Fast Scanning Probe upstream and outer divertor domed Langmuir probe measurements indicate that the EDA H-mode is in the High Recycling Divertor regime [2], where the measured electron pressure is approximately constant along the field, but the electron temperature falls between the upstream location and the divertor plate. The EDA H-
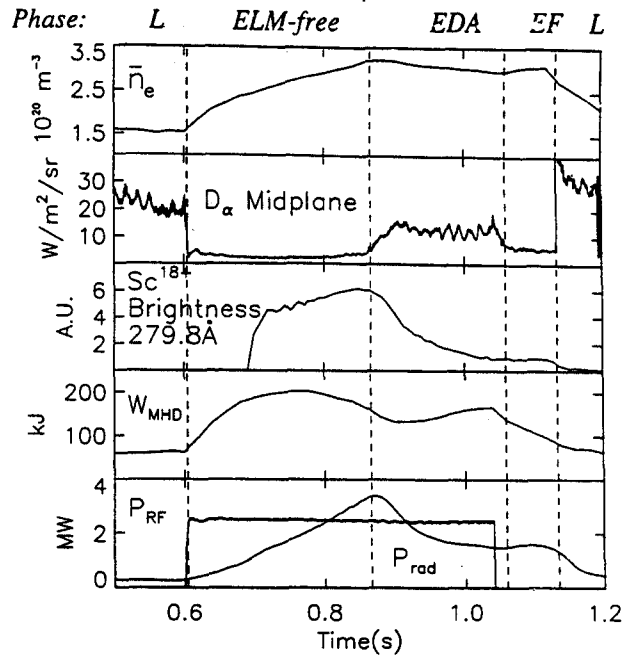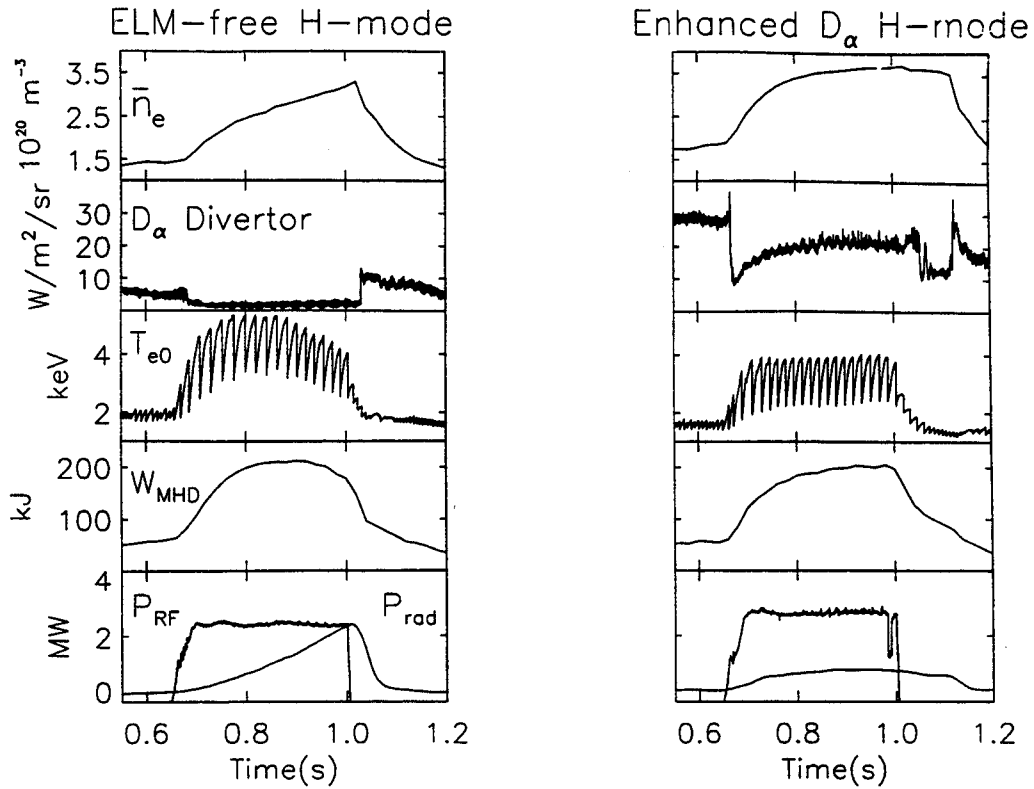
14

Fig. 2. Comparison of a) ELM-free H-mode and b) Enhanced D_α H-mode showing the line averaged density, divertor D_α emission, central electron temperature, stored energy, total radiated power and ICRF power.

mode occurs at high density when the power conducted to the divertor plate is sufficiently high (Fig. 3). Here $P_{plate} = P_{in} - dW/dt - P_{rad}^{main} - P_{rad}^{div}$ is the power that arrives at the divertor plate after subtracting the change in stored energy and both main chamber and divertor radiation. Figure 3 shows an EDA H-mode that turns into a detached divertor H-mode through intense nitrogen gas puffing. The enhanced D_α emission returns to ELM-free levels when the power conducted to the plate drops due to increased radiation, just as the divertor detaches.

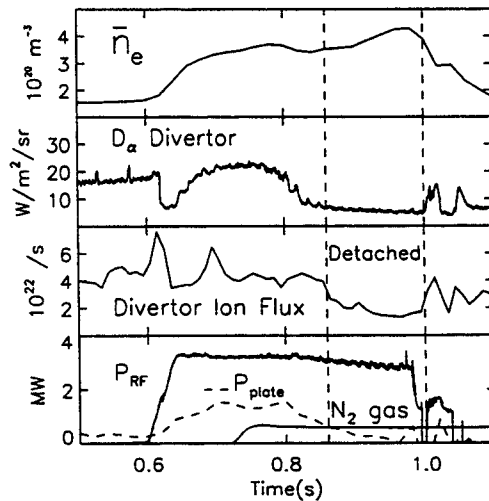**Edge Fluctuations** High frequency magnetic and density fluctuations are often observed during EDA H-mode.

Fig. 3. Detached divertor H-mode with nitrogen puffing. The D_α emission is suppressed as the power to the plate drops.

The magnetic perturbations are covered in a companion paper in these proceedings [3]. The density fluctuations are observed with an AM reflectometer at 88 GHz with a density cutoff in the steep gradient region at 1.5×10^{20} m^{-3}. In EDA H-mode, there is an increase in the broadband fluctuations out to the 400 kHz anti-aliasing filter of the diagnostic and often
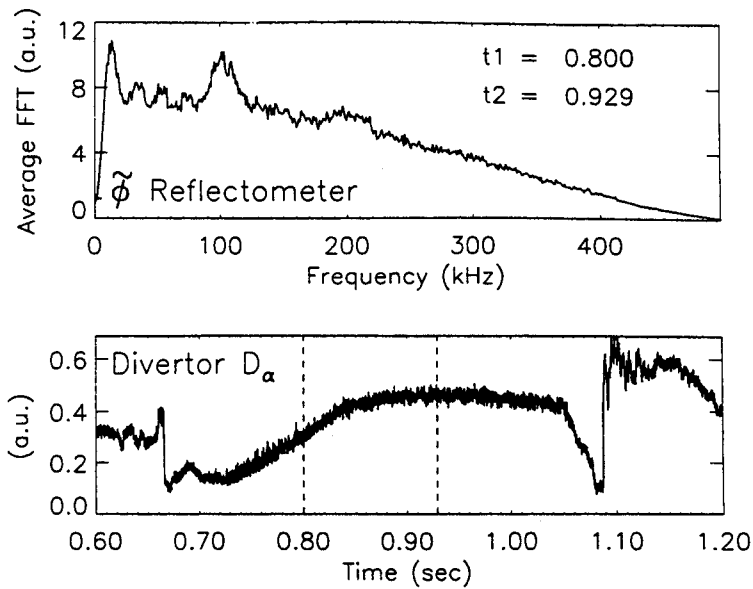

Fig. 4. Average between 0.8 and 0.929 sec of the Fourier transform of the density phase fluctuations from the reflectometer during an Enhanced Da H-mode showing a clear peak in the fluctuations at about 100 kHz.

an additional coherent peak at typically 100 kHz (Fig. 4). Although the magnetic fluctuations are often at about the same frequency and time, there is no clear coherence between the magnetic and density fluctuations.

Conclusion The Enhanced D_α H-mode regime may prove to be a good compromise for ITER operation to obtain high confinement, avoid large ELMs, and maintain low Z_{eff} with high divertor radiation in steady state. In comparison with ELM-free H-modes, impurity accumulation is substantially reduced in EDA H-modes leading to lower Z_{eff} values and lower total radiated power across the main plasma and a factor of two higher radiated power in the divertor. The energy confinement is comparable in both types of H-mode. High frequency edge density and magnetic fluctuations are observed during EDA H-mode, though the role they play has not yet been determined.

References

[1] Y Takase, et al., Phys. Plasmas 4 (1997) 1647.

[2] B LaBombard, et al., Phys. Plasmas 2 (1995) 2242.

[3] I H Hutchinson, et al., this conference.

Analysis of ICRF Heating on Alcator C-Mod*

Y. Takase, P. Bonoli, S. Wukitch, C. Fiore, A. Hubbard,

A. Mazurenko, P. O'Shea, M. Porkolab, J. Reardon, C. Rost

MIT Plasma Science and Fusion Center, Cambridge, Massachusetts 02139 U.S.A.

1. Introduction

Alcator C-Mod [1] ($R = 0.67$ m, $a = 0.22$ m, lower single-null, $\kappa = 1.7$ typical) is a compact high field tokamak. The first wall consists of all metallic (mostly molybdenum) plasma facing components. Experiments described in this paper were performed with boronized walls. The heating scenario employed was hydrogen minority heating in deuterium majority plasmas at 5.3 T with RF powers in the range 1.5–3 MW at 80 MHz [2,3].

2. Power absorption in L-mode plasmas

A density scan at an RF power level of 1.5 MW was performed in L-mode plasmas. In order to avoid H-mode at this power level, the toroidal field was reversed so that the ion ∇B drift was directed away from the active X-point. The density scan was repeated at two values of plasma current, 0.8 MA and 1.1 MA (the density range for the 1.1 MA scan was limited to $\bar{n}_e > 1.6 \times 10^{20}$ m^{-3}). The hydrogen concentration was less than 3%.
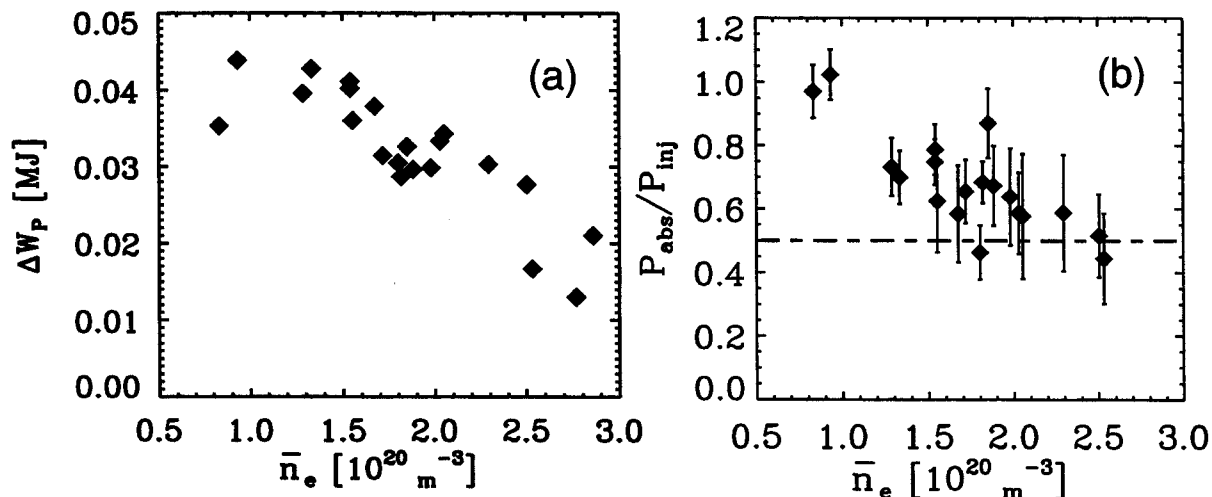
Fig. 1: (a) Stored energy increase and (b) power absorption efficiency as functions of density. L-mode plasmas, $B_T = 5.3$ T, $I_p = 0.8$, 1.1 MA, $n_H/n_e \leq 3\%$, $P_{RF} = 1.5$ MW.

Heating, as measured by the stored energy increase ΔW, degrades by roughly a factor of two as the density is increased as shown in Fig. 1(a). The absorption efficiency, estimated from the discontinuity in slope of the diamagnetic stored energy, also

---

degrades with density from 100% to 50%, as shown in Fig. 1(b). The incremental con-finement time, $\Delta W/\Delta P$ is approximately constant at 0.045 s. The heating degradation at higher density is therefore attributed to lower power absorption efficiency. The cause of degraded absorption efficiency for high density L-mode plasmas is presently not well understood, but may be related to the higher edge plasma and neutral densities. In contrast, power absorption in high density ($\bar{n}_e > 3 \times 10^{20}\,\mathrm{m}^{-3}$) H-mode plasmas is nearly 80%.

3. Power absorption profiles

In D(H) minority heating, most of the RF power is absorbed by the hydrogen minority ions. Electrons and bulk deuterium ions are heated by collisional power trans-fer from the heated hydrogen minority ions. A small fraction of the RF power can be absorbed directly by the majority deuterium ions by second harmonic damping. The central electron heating rate can be derived from the central electron reheat rate after a sawtooth crash. The contribution from the ohmic heating power must be subtracted to obtain the contribution from RF heating. The central ion heating rate can be measured from the discontinuity in slope of the central ion temperature. Both the central electron heating rate and the central ion heating rate increase with density, as shown in Fig. 2. The increase of the central electron heating rate with density may be counter-intuitive, but this can be explained by the more localized power deposition at higher density. The central (averaged over $r/a \leq 0.25$) power transfer densities to electrons and ions calcu-lated by TRANSP[4]/FPPRF[5]/SPRUCE[6] are shown for comparison. The fraction of power transferred to electrons averaged over the whole plasma volume (compared to power transferred to bulk ions) does decrease with density.
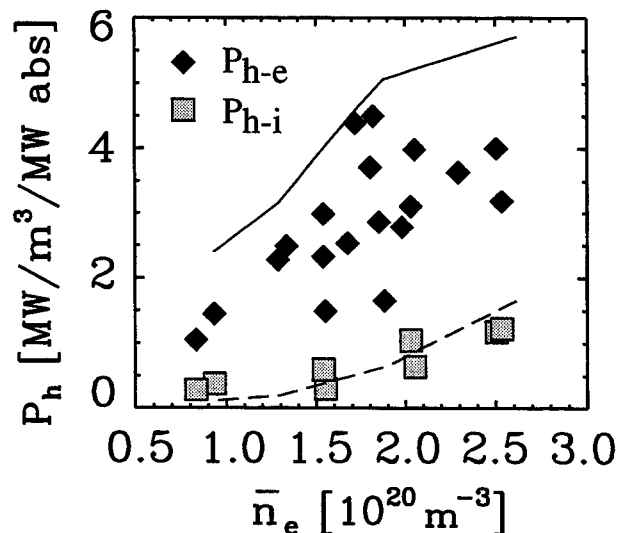

Fig. 2: Central electron and ion heating power densities as functions of density. Same parameters as Fig. 1. The solid line and the dashed line are central electron and ion heating power densities calculated by TRANSP/FPPRF/SPRUCE.

There are two mechanisms responsible for localization of power deposition at higher density. The first is the wave focusing effect. At higher densities the radial wavelength of the fast wave becomes small compared to the minor radius of the plasma, and the wave field becomes more tightly focused. At lower densities the radial wavelength becomes comparable to the minor radius and diffraction becomes important. This effect will determine the power deposition width in the vertical direction along the cyclotron resonance. The second effect is due to Doppler broadening of the ion cyclotron resonance in the horizontal direction. At lower densities the average energy of the minority ions becomes larger, thus increasing the radial width of power deposition. A comparison of power absorption contours calculated by the FPPRF/SPRUCE code for low density and high density plasmas are shown in Fig. 3. Because the vertical extent is generally larger than the horizontal extent, power deposition width is determined mainly by the wave focusing effect.
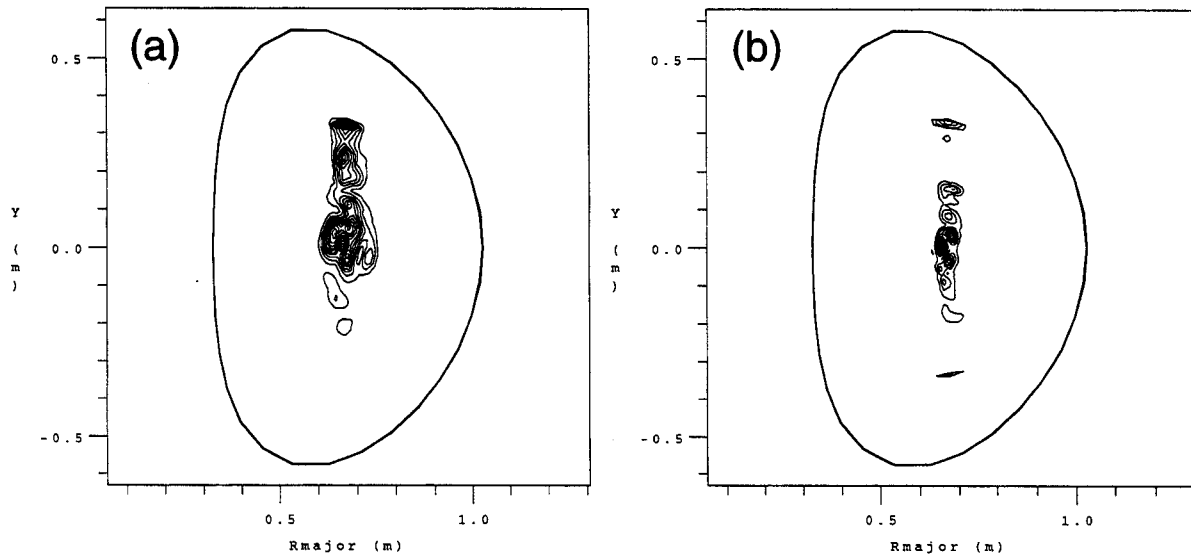

Fig. 3: Total power absorption contours at two densities: (a) $\overline{n}_e = 0.9 \times 10^{20}\,\mathrm{m}^{-3}$, *(b)* $\overline{n}_e = 2.6 \times 10^{20}\,\mathrm{m}^{-3}$. *Same parameters as Fig. 1.*

The energy stored in the energetic minority ions is 30% of the total stored energy at the lowest density in this scan, but decreases to 5% at the highest density. At the lowest density in this scan, fast ion orbit loss is calculated to be significant (about 20% of the absorbed RF power), but is negligible at higher densities.

4. Second harmonic damping

In high power H-mode plasmas, β of the main ions becomes significant. The central ion beta of $\beta_{i0} = 1.5\%$ has been obtained at 5.3 T. Under such a condition, second harmonic damping on the majority deuterium ions can dominate over hydrogen minority ions for low hydrogen concentrations. Calculations show that switch-over to dominant second harmonic deuterium damping takes place for $n_H/n_e \leq \beta_{i0}$, as shown

in Fig. 4 where the central (integrated up to $r/a \leq 0.35$, the sawtooth inversion radius) power absorption by second harmonic deuterium, fundamental hydrogen, and mode conversion are plotted for a high-density high-power H-mode as functions of hydrogen concentration n_H/n_e. Such concentrations have been achieved after an extended period (1–2 months) of deuterium plasma operations. Second harmonic deuterium heating may be useful for enhancing the fusion reactivity in high performance plasmas such as high power, high density H-mode or PEP mode plasmas[3].
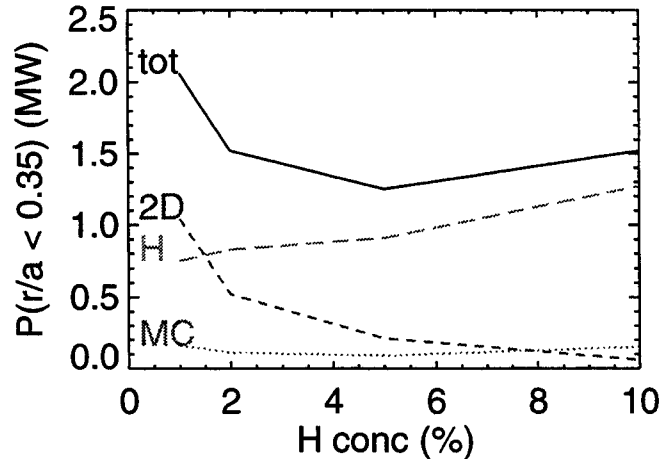

Fig. 4: *Central power absorption by second harmonic deuterium, fundamental hydrogen, and mode conversion in high-density high-power H-mode as functions of hydrogen concentration n_H/n_e. $B_T = 5.3\,T$, $I_p = 1.0\,MA$, $P_{RF} = 2.7\,MW$, $\bar{n}_e = 4.2 \times 10^{20}\,m^{-3}$.*

5. Conclusions

A degradation of heating (stored energy increase) was observed in high density L-mode plasmas, which was attributed to a degradation of the absorption efficiency by a factor of 2. In high density H-modes, power absorption was substantially higher (nearly 80%). Both central electron and ion power densities increased with density due to more localized power absorption. In high density H-mode plasmas, second harmonic absorption can become important at low hydrogen concentrations $n_H/n_e \leq \beta_{i0}$.

References

[1] I.H. Hutchinson, et al., Phys. Plasmas 1, 1511 (1994).

[2] Y. Takase, et al., Plasma Phys. Control. Fusion 38, 2215 (1996).

[3] Y. Takase, et al., Phys. Plasmas, 4, 1647 (1997).

[4] R. J. Hawryluk, in *Physics of Plasmas Close to Thermonuclear Conditions*, Vol. 1 (CEC, Brussels 1980) p. 19.

[5] G. W. Hammett, Ph. D. Thesis, Princeton University (1986).

[6] D. N. Smithe, et al., Nucl. Fusion 27, 1319 (1987).

Volume Recombination in Alcator C-Mod Divertor Plasmas

J.L. Terry, B. Lipschultz, D. Lumma, B. LaBombard, and D. Pappas
Plasma Science and Fusion Center, MIT, Cambridge, MA, 02139, USA

1 Introduction

Volume recombination has been predicted to be a significant process in tokamak divertors under detached conditions. These predictions arise from a number of considerations - from modelling [1,2], as the mechanism for removing a large fraction of ion flux [3,4,2], and as a probable consequence of the ~1 eV electron temperatures observed in the detached divertor plasmas of DIII-D [5] and Alcator C-Mod[6]. The first experimental measurements of significant volume recombination in a tokamak divertor were on Alcator C-Mod[7], where the ion sink due to recombination was observed to be comparable to the ion loss to the plates. In addition, recent measurements on a linear device[8] have also shown the importance of recombination during simulations of plasma detachment. The observations are consistent in a broad sense with the theoretical considerations and modelling. However, more detailed experiments and comparisons with the modelling are required before the role of recombination in the physics of plasma detachment is understood and can be exploited to achieve the heat and momentum dissipation required in future fusion reactors.

In this paper a more streamlined analysis technique, which relates the number of recombinations occurring within a field-of-view to the number of Balmer series photons emitted within that view, is presented. This technique is then exploited to determine the spatial distribution of the volume recombination occurring in the Alcator C-Mod divertor region when the inner divertor plate is detached, while the outer divertor plate is still attached.

2 Recombinations per Balmer Series Photon

For the determination of the recombination rates in Alcator C-Mod, measurements of the Balmer series lines of D_0 are used. An example of such a spectrum, containing the $n=6,7,8...11 \rightarrow 2$ lines is shown in Fig. 1. Measurements of D_α ($n=3\rightarrow2$) along the same view are also made at the same time. From the spectra it is apparent that the Balmer lines are Stark broadened, with line widths, consistent within a given spectrum, which correspond to electron densities as high as $\sim 2 \times 10^{21} \mathrm{m}^{-3}$. In addition, the measurements typically show that the scaling of the upper level population densities of these transitions is consistent with a population distribution which is a result of recombination. They are inconsistent with population by excitation. This can be shown using a collisional-radiative model like that of Johnson and Hinnov[9] or Fujimoto et al. [10]. Since the scaling of the observed line brightnesses is that of population-by-recombination, the same collisional - radiative model has been employed to relate the volume emission rate of those measured lines to the total volume recombination rate, as long as the electron density and temperature are also known. The number of recombinations per photon of any Balmer series line has been calculated vs T_e and n_e for a recombining plasma. ($n_e = n_i$ is assumed.) This is the recombination analog for what Johnson and Hinnov [9] have done in the *ionizing* case, where curves showing the number of ionizations per D_α photon for an ionizing plasma were generated. We have generated curves which give the number of
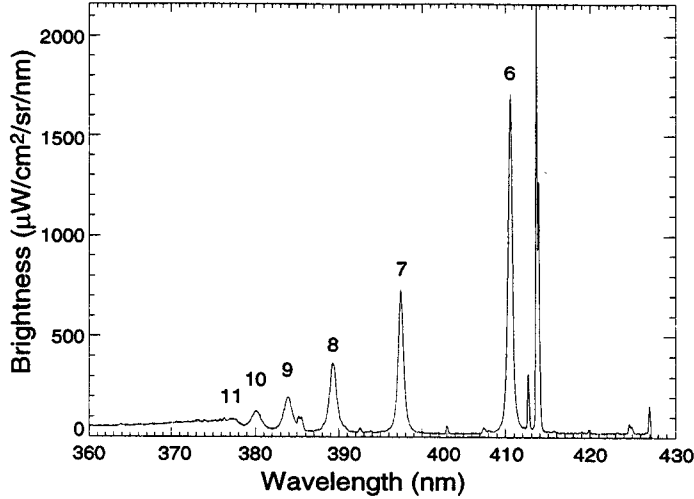
Figure 1: *The higher n D_0 Balmer series lines (n=11, 10, ...6 → 2). The widths of the Stark broadened lines correspond to a density of ~ 1.5×10^{21} m^{-3}. The view for this spectrum is of the inner, detached divertor plate.*

recombinations per Balmer-series-line photon, with the condition that the upper level of the line be populated by recombination. Examples of this quantity vs T_e are shown in Fig. 2 at two different densities. Here we have used the model of Ref. [10], although use of Ref. [9] gives essentially the same results.
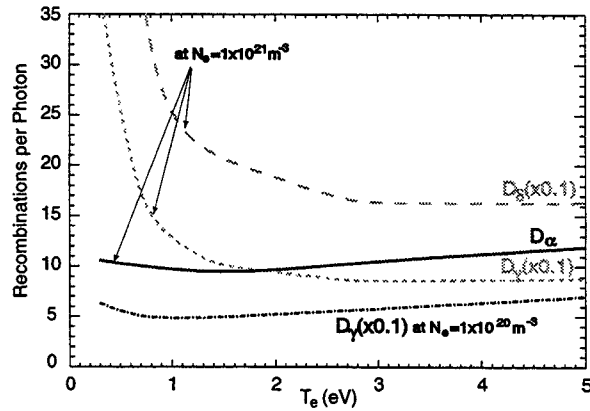
Figure 2: *The number of recombinations per photon for three Balmer series lines, calculated in a recombining plasma and showing the relatively weak T_e dependence for $T_e \gtrsim$ ~0.8 eV. $n_e = 10^{21}$ m^{-3} and 10^{21} m^{-3} for the second D_γ curve.*

3   Spatially Resolved Measurements of Recombination

In order to provide more detailed measurements of the connection between recombination and detachment, we have used the formalism described above to analyse the spatial distribution of the recombination during an Alcator C-Mod discharge when the inner divertor

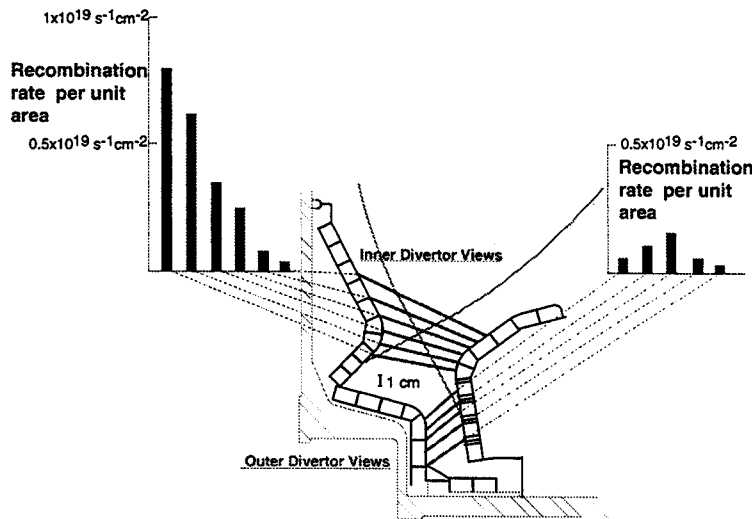Figure 3: *The recombination rate per unit area determined for different viewed areas of the inner and outer divertor plates. The inner divertor plate is detached, while the outer is not. Also shown are the viewing chords, the LCFS, and the strike points.*

plate was detached, but the outer plate was not. Other plasma parameters were I_p=1.0 MA, P_{ICRF}=1 MW, $\overline{n_e}$ = 3.5 × 10^{20}m^{-3}, with H-mode confinement. The line brightnesses of the n=3,6-11 → 2 are measured along the viewing chords (with diameters of ~1cm) shown in Fig. 3. The chords have diameters of ~ 1 cm. Radial profiles of D_α emission, measured from a separate array, viewing the divertor from above, show that the emission is is strongly peaked between the inner divertor plate and the x-point, but falls to about 20% of its peak value along the outer (attached) divertor plate. These measurements lead us to ascribe the photons detected by those views to recombination occurring near the inner divertor. Similarly, we take the measured D_0 emission along the chords labeled 'outer-divertor-view' to be due to recombination at the outer plate. After verifying that the Balmer lines (n=3, 6, 7 → 2) exhibit the characteristic recombination scaling with n, curves similar to those of Fig. 2 (but generated for the plasma densities measured from the line widths) are used to measure the recombination rate per unit area of plasma surface viewed. Since the recombinations per photon varies little with T_e at higher temperatures, the T_e needed for the evaluation is only an issue if it is $\lesssim 0.8$ eV, in which case the ratio between the 3-2 and 6-2 lines can be used to estimate the temperature. In fact all of the analyses are consistent with $T_e \gtrsim 0.8$ eV. The results of the evaluations are also shown in Fig. 3. The 'inner-divertor-views' show that the recombination increases as the inner - detached - strike point is approached. The more extensive array of D_α views shows that the emission, and, by implication, the recombination rate are peaked at or close to the strike point. However, rates for those views are not shown, since the other Balmer lines were not measured. The integration providing the total recombination rate in front of the inner plate has been done after interpolating poloidally between the views by assuming toroidal symmetry. This 'inner plate' recombination was then compared to the rate at which ions were being collected at the plate, measured by a set of five probes embedded in the inner plate. The recombination rate ($\sim 2.7 \times 10^{22}$ s^{-1}) is approximately a factor of two greater than the ion current ($\sim 1 \times 10^{22}$ s^{-1}) to this detached plate. The

23

time histories of each rate show that this ratio stays fairly constant for the entire time the inner plate is detached, which is essentially the duration of the diverted discharge. An analogous evaluation has also been done for the outer - attached - plate. As shown, the recombination is much reduced here, although the rate is similarly peaked close to the outer strike point. The ion current collected by the outer plate ($\sim 4 \times 10^{22}$ s^{-1}) is about 20 times the recombination rate there.

4 Summary and Discussion

Significant volume recombination of the majority ions is been observed in the divertor region of Alcator C-Mod under detached conditions. This determination is made by analysis of the visible spectrum from the divertor, in particular the Balmer series line emission. After verification that the upper levels of the measured lines are populated primarily by recombination, the recombination rate within the field-of-view has been found from curves relating the number of recombination per Balmer-series-line photon. These curves are relatively insensitive to T_e and n_e, although n_e is measured from the Stark-broadened line-widths. The distribution of the recombination is found for a case where the inner divertor plate is detached, while the outer plate is not. The recombination rate in the detached region in front of the inner divertor plate is approximately a factor of two higher than the rate of ion collection at the plate. For the attached plate, the recombination occurring in front of it is still small in comparison to the ion current to the plate. For both plates the recombination is peaked near the strike points. This may be a result of the fact that at this time for this discharge n_e is highest and T_e lowest at the strike point locations. It is interesting also to speculate about the effects of the detached/attached asymmetry between the plates and the resulting, observed asymmetries in recombination and ion currents. We note that the total ion sink (recombination plus ion current) is still approximately balanced between the plates, so that neutral density made up of recombined *and* recycled neutrals may be balanced as well. It is still possible, however, that differences in neutral density distributions may arise due to the volume source nature of recombination. Such differences may give rise to complicated ion/neutral flow patterns in the SOL.

Finally, we discuss the possible opacity of Lyman series lines. The analysis and Fig. 2 assume that all lines are optically thin. In fact, Ly$_\alpha$ is probably thick along some paths, and there is evidence on other, higher density shots that Ly$_\beta$ is somewhat self-absorbed. The Balmer series lines are optically thin. The greatest effect of Ly$_\alpha$ self-absorption will be an enhancement of the $n=2$ level and a possible over-estimate of the recombination rate.

References

[1] F. Wising et al., Contrib. Plasma Phys. 36, p 136 (1996)

[2] S.I. Krasheninnikov et al., Phys Plasmas 4, p 1638 (1997)

[3] A. Loarte, Proc. 12th PSI Conf, J. Nucl. Mater (1996) I9, in press

[4] K. Borrass et al., Proc. 12th PSI Conf, J. Nucl. Mater (1996) A41, in press

[5] S. L. Allen et al., Proc. 12th PSI Conf, J. Nucl. Mater (1996) B37, in press

[6] B. LaBombard et al., Phys Plasmas 2, p 2242 (1995)

[7] D Lumma et al, Phys Plasmas (1997), in press

[8] J. Park et al., submitted to PRL 1997

[9] L.C. Johnson and E. Hinnov, JQSRT 13, p 333 (1973)

[10] T. Fujimoto et al., Nucl Fus 28, p 1255 (1988)

An Analysis of the H-mode Threshold in ITER
The ITER H-mode Threshold Database Working Group
presented by J A Snipes*

MIT Plasma Science and Fusion Center, Cambridge, MA USA

Introduction Attempts have been made for several years to accurately predict the threshold power required to achieve H-mode in ITER [1-2]. These studies have concentrated on regression fits to global quantities, with the line averaged density, toroidal field, major radius, aspect ratio, and elongation as the dominant terms. This paper extends these analyses to the most recent ITER H-mode Threshold Database DB2.2, which includes more than 5000 time slice records each with 156 variables from Alcator C-Mod, ASDEX-Upgrade, Compass, DIII-D, JET, JFT-2M, JT-60U, and TCV. In addition, more than 600 records of older data are included from the previous DB2 version of the database from ASDEX and PBX-M. The new database includes global quantities as well as local edge temperature and density measurements at the 90% and 95% flux surfaces under a variety of plasma conditions including ohmic, ICRF, and neutral beam heating. More attempts have been made to reduce the scatter in the data from many tokamaks with very different first wall properties to try to reduce the uncertainty in the threshold power predicted for ITER. The main reasons for scatter in the data vary for different machines including the step size of the input power, the change in stored energy, and neutral particle effects. Recent work suggests that sawteeth may play an important role in the threshold and could also increase scatter in the data. The result is that there remains a large uncertainty in predicting the threshold power for ITER.

Global Analyses The threshold power required to achieve H-mode can vary by more than a factor of two within a tokamak. So, one approach is to include only H-mode threshold points that have no known reason for having an unusually high threshold power and flagging them as SELDB2 = 1111111111. Using these standard selection criteria and performing the usual n, B, and R regression on the latest dataset with equal weighting between points from all 10 tokamaks (N=518) yields (Fig. 1):

$$P_L = P_{in} - \frac{dW}{dt} = 0.65 \cdot \bar{n}_e^{0.93} \cdot B_T^{0.86} \cdot R^{2.15} \quad \text{(Eq. 1)},$$

where the power is in MW, the line averaged density is in units of 10^{20} m^{-3}, the toroidal field is in Tesla, and the major radius is in m. This analysis yields a predicted threshold power in ITER of P_{th}(ITER) = 139 MW, using a line averaged density of 0.5×10^{20} m^{-3}, B_T = 5.68 T, and R = 8.14 m, with a one standard deviation uncertainty interval of about 107 to 182 MW,

assuming the model is correct and the main engineering variables that influence the threshold power are included.

Alternatively, if the elongation of the plasma is included as a regression variable with the same selection criteria, the following threshold scaling is found (Fig. 2):

$$P_L = 0.42 \cdot \bar{n}_e^{0.80} \cdot B_T^{0.90} \cdot R^{1.99} \cdot \kappa^{0.76} \qquad \text{(Eq. 2)},$$

which yields a predicted threshold power for ITER of 108 MW and a one standard deviation uncertainty interval of about 78 to 151 MW. This point prediction is close to that of Takizuka [2]. If the points are weighted so that each tokamak carries equal weight, W = $1/N_j$, where N_j is the number of data points from tokamak j, the scaling becomes:

$$P_L = 0.67 \cdot \bar{n}_e^{1.07} \cdot B_T^{0.73} \cdot R^{2.17} \cdot \kappa^{0.44} \qquad \text{(Eq. 3)}.$$

With this scaling, the predicted threshold power for ITER is 131 MW with an uncertainty interval of 92 to 187 MW. Note that each of these regressions was performed as a free fit, yet all except Eq. 3 came out very close to satisfying the Kadomtsev constraint [3]. Each of these predicted thresholds falls within the 50 - 200 MW range predicted by Takizuka.

One attempt to further reduce scatter in the data has been to specify an "ITER Oriented" dataset, which includes elongations from $1.4 < \kappa < 1.8$ and safety factors from $2.8 < q_{95} < 4.0$. This severely restricts the data in the database (N=221), and eliminates ASDEX, DIII-D, PBX-M, and JFT-2M. The uncertainties do not decrease and the point predictions for equal weighting between points, 102 MW (1σ = [72 - 147] MW), or between tokamaks, 112 MW ([78-161] MW), remain in the same range as the previous scalings.

Another potentially important effect to consider is the radiated power. Due to the lack of reliable radiated power measurements from within the last closed flux surface, Compass, PBX-M, and TCV are eliminated when radiated power is subtracted from the input power. The resulting regression fit between the remaining seven machines (N=142) with W = 1/N gives $P_L - P_{rad} = 0.35 \, n_e^{0.73} \, B_T^{0.94} \, R^{2.27}$, which is not very different from the expression without subtracting radiation and yields nearly the same threshold prediction for ITER of 124 MW with a larger uncertainty interval of [77 - 200] MW because of the smaller dataset and the increased uncertainty due to the inclusion of radiated power measurements.

Local Analyses Another approach to the threshold is to consider local edge measurements instead of global ones since some machines have found a dependence of the H-mode threshold on edge conditions, most notably the electron temperature. New data was added to the DB2.2 version of the threshold database including temperatures and densities at the flux

26

surfaces corresponding to 90% and 95% of the square root of the toroidal flux. Due to the difficulties in obtaining accurate edge temperature and density measurements, Compass and JFT-2M were eliminated from the analysis and the scatter in the data from the remaining machines leads to large uncertainties in any predictions based on the edge measurements.

Nonetheless, an attempt was made to predict the edge electron temperature at the H-mode threshold in ITER. The best fits were obtained regressing $T_e(95)$ and $T_e(90)$ as functions of toroidal field, line averaged density (statistics were poor using $n_e(95)$), q_{95}, and major radius. The results with equal weighting between points are (Figs. 3-4):

$$(N=62) \qquad T_e(95)(eV) = 126.38 \cdot B_T^{1.32} \cdot \bar{n}_e^{-0.5} \cdot R^{0.56} \cdot q_{95}^{-1.31} \qquad \text{(Eq. 4)}$$

$$(N=102) \qquad T_e(90)(eV) = 170.29 \cdot B_T^{1.02} \cdot \bar{n}_e^{-0.3} \cdot R^{0.74} \cdot q_{95}^{-0.94} \qquad \text{(Eq. 5)}.$$

The predictions for ITER are then $T_e^{ITER}(95) \approx 1250$ eV, with a one standard deviation uncertainty interval of about 500 eV to 3200 eV, and $T_e^{ITER}(90) \approx 2000$ eV, with an uncertainty interval of 950 eV to 4200 eV. The L-mode gradient is then predicted to be about 6 keV/m, which is somewhat low compared to existing devices. This scaling has the same density dependence but a stronger plasma current dependence and a weaker toroidal field dependence than the recent scaling found on ASDEX-Upgrade for edge T_e in terms of edge n_e [4]. Assuming the transition is governed only by plasma physics and that atomic physics can be neglected, the criterion for a transition should have the form

$\rho_*^x \cdot v_*^y \cdot \beta^z = const.$ [3,5] and the exponents in the edge temperature scalings should satisfy the constraint $8\alpha_n - 4\alpha_R + 5\alpha_B = 2$. Eqs. 4 and 5 do not satisfy this constraint to within an exponent of 2. So, either the assumptions are incorrect or the regression has not found the correct dependences within this limited dataset.

Conclusions Despite continued attempts to reduce the uncertainties in the prediction of the H-mode threshold power in ITER, large uncertainties remain with global predictions in the range of 50 - 200 MW. Narrowing down the selection criteria results in poorer statistics with equally large or larger uncertainties than using the full dataset. The observed variation in threshold power in existing machines must also be expected in ITER. New analysis of the edge electron temperature at the H-mode threshold predicts $T_e^{ITER}(95) \approx 1250$ eV with edge gradients on the order of 6 keV/m.

DB2 H-mode Threshold Power Scaling

RMSE (%) = 27.4
P_{ITER} (MW) = 139
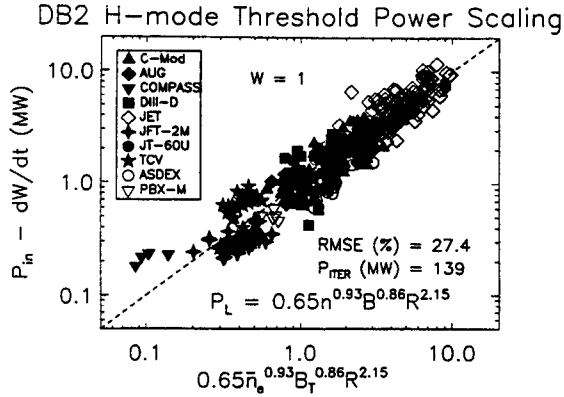
$$P_L = 0.65n^{0.93}B^{0.86}R^{2.15}$$

Fig. 1. Standard regression of the H-mode threshold power versus line averaged density, toroidal field, and major radius with equal weighting between points.
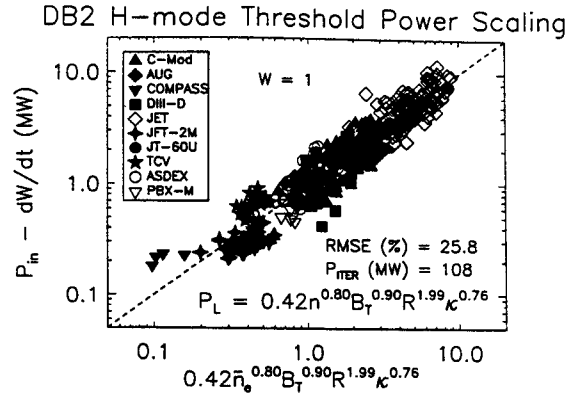
DB2 H-mode Threshold Power Scaling

RMSE (%) = 25.8
P_{ITER} (MW) = 108

$$P_L = 0.42n^{0.80}B_T^{0.90}R^{1.99}\kappa^{0.76}$$

Fig. 2. H-mode threshold power regression including plasma elongation across 10 tokamaks with equal weighting between points.

Edge T_e H-Mode Threshold Power Scaling

T_{e95}^{ITER} (eV) = 1254
RMSE = 19.3%

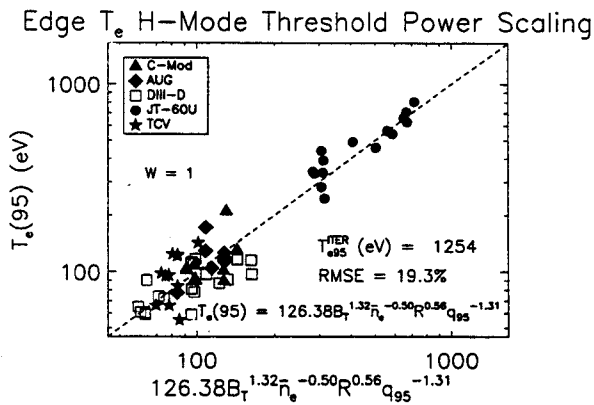$$T_e(95) = 126.38B_T^{1.32}\bar{n}_e^{-0.50}R^{0.56}q_{95}^{-1.31}$$

Fig. 3. Edge electron temperature regression at the 95% flux surface versus toroidal field, line averaged electron density, and edge safety factor.

Edge T_e H-Mode Threshold Power Scaling

T_{e90}^{ITER} (eV) = 1991
RMSE = 22.0%

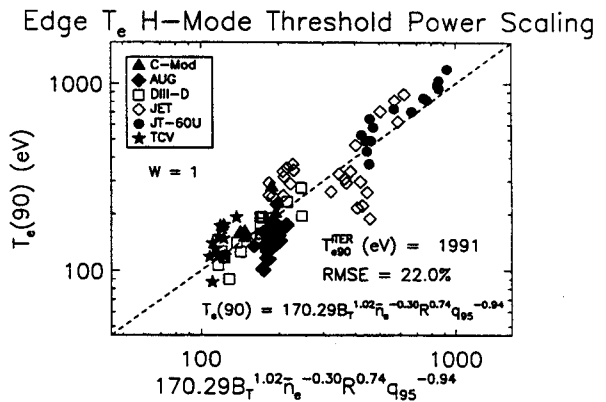$$T_e(90) = 170.29B_T^{1.02}\bar{n}_e^{-0.30}R^{0.74}q_{95}^{-0.94}$$

Fig. 4. Edge electron temperature regression at the 90% flux surface versus toroidal field, line averaged electron density, and edge safety factor.

References

[1] F Ryter, H-Mode Database Working Group, *Nuclear Fusion,* **36** (1996) 1217.

[2] T Takizuka, et al., in *Plasma Physics and Cont. Nucl. Fus. Res. 1996 (Proc. 16ᵗʰ IAEA Conf., Montreal, 1996),* to be published.

[3] B B Kadomtsev, *Sov. J. Plasma Phys.,* **1** (1975) 295.

[4] W Suttrop, et al., to be published in *Plasma Physics and Controlled Fusion.*

[5] J W Connor and J B Taylor, *Nuclear Fusion,* **17** (1977) 1047.